International Journal of Engineering Trends and Technology
ISSN: 2231–5381 / https://doi.org/10.14445/22315381/IJETT-V73I9P110

Volume 73 Issue 9, 100-113, September 2025

Original Article

Enhanced Glaucoma Detection in Fundus Images Using CNNs with Retinex and Color Correction

Upasana Mishra[1*,2], Jagdish Raikwal[3]

[1*,3]*Institute of Engineering & Technology, Devi Ahilya University, Indore, Madhya Pradesh, India.*
[2]*Apex Institute of Technology, Chandigarh University, Mohali, Punjab, India.*

[1*]*Corresponding Author : upasna.tiwari10@gmail.com*

Received: 28 April 2025 Revised: 01 September 2025 Accepted: 13 September 2025 Published: 30 September 2025

Abstract - *Glaucoma leads to an unequivocal, irreversible blindness all over the world. In 2020, there were an estimated 80 million glaucoma cases. Complex screening methods and a lack of human resources create delays that are contributing to global vision loss. An automatic, efficient system for the detection of the affected area of glaucoma should be designed, which will overcome the drawbacks of manual methods. Most existing machine learning algorithms are primarily used as a prediction tool, which makes it difficult for doctors, patients, and other practitioners in the medical field to understand how the data is processed for analysis and decision-making. In this article, a CNN-based Retinex framework with a colour correction method is developed to overcome these issues. The proposed method combines the CNN and general loss function and color correction for improving the appearance of fundus images to restore the original colors and remove the illumination effects. Methods: This method uses statistical tests in dataset preprocessing. The framework is presented with concrete diagrams and mathematical notation, which will lead to reproducible results. The framework developed here, in conjunction of demonstration, may be expanded to automated diagnostic tools for glaucoma for use in clinical practice.*

Keywords - *Convolutional Neural Network, Color Correction Algorithm, Deep Neural Network, Glaucoma Detection, Retinex.*

1. Introduction

Glaucoma is an incurable eye condition that can only be delayed by medication and surgical therapies. Existing glaucoma detection methods are unreliable. Manual glaucoma identification (i.e., optic nerve head assessment) is subjective, costly, time-consuming, and physician competence varies widely. Several automated glaucoma detection processes using color fundus images have been developed. At present, the methods that are currently used to detect glaucoma do not reliably produce results that are sufficient. Manual glaucoma identification, also known as an examination of the optic nerve head, is a subjective process that is also an expensive and time-consuming process. Additionally, there is a significant amount of variation in physician performance. Glaucoma screening from fundus images is challenging due to illumination/color variations among fundus images and the early stage of the disease. This decreases separability and results in overestimating false positives in the classical CNN pipeline. The aim of this paper is to fill this gap by combining "color augmentation" implemented with Retinex-based illumination normalization, to explicitly color Enhancement before learning, and by statistics-based ROI selection to a compact CNN trained with generalized cross-focal loss, which can address class imbalance. This ordering renders inputs stable, bringing out clinically relevant regions and sharpening decision boundaries. Unlike the previous Pipeline, which lacks illumination correction or low-level CNNs that misclassify early cases, our Pipeline combines the Retinex and ROI in a pre-CNN stage and validates each module by ablations (policies 1-4), quantitative hypothesis testing and rigor.

This paper also observes improvements in sensitivity, specificity, and Accuracy when both channels and regions of interest are utilized, and the full model outperforms the baselines in recall, Precision, Accuracy, and mAP@0. 75. In this paper, place these options in recent literature, and surface dataset scale/splits to support comparisons. In prior work, researchers revealed that a number of automated procedures for the diagnosis of glaucoma based on color fundus pictures are being considered for the role. Work done since 2002 includes [1-9]. Since 2020, recent work includes [10-15].

All of the studies on glaucoma detection methods that have been listed above are based on machine learning techniques. Some of them use color fundus images as input data. Data categorization and data transformation are the two main phases in these processes. When the source data are colour fundus pictures, transforming them into transformed data is called data transformation. The process is called data classification when the binary output is a diagnosis of glaucoma or a

healthy eye. Automatic glaucoma diagnosis has been created by [2] using a convolutional neural network and other components of DL architecture. As a deep learning system example, CNNs can differentiate glaucoma patterns from non-glaucoma patterns to make diagnostic choices. The use of CNNs for automated diagnosis of eye fundus photographs was shown in [3]. The advantages and disadvantages of AI-enabled glaucoma detection frameworks that use segmented fundus pictures were analyzed and summarized in a review [11]. XAI and Interpretable ML (IML) models were created by Kamal et al. to assess glaucoma forecasts and outcomes. Kamal et. al [14], PDA and the ANFIS are the main technologies used by XAI to give credible explanations for glaucoma predictions produced using infected and healthy images[14].

Automated glaucoma finding using deep learning that accounts for OD and OC localization [16]. To identify glaucoma and evaluate visual function using retinal structures, [17], created an end-to-end attention-driven 3D deep learning model. An attention-based CNN technique for glaucoma diagnosis was described in [18, 19]. AG-CNN. Specifically, a massive LAG database was built. [20], created a multi-task CNN that segments the OD and the OC from colour fundus images and predicts the presence of glaucoma. Image processing and ML for organization have been considered for detecting glaucoma [21].

In [22], the use of a deep CNN for glaucoma detection was reported. This paper presents AT-GICD for classifying glaucoma in eye images, using advanced techniques like image segmentation, histogram enhancement, and wavelet energy features. The approach then leverages ANN to distinguish between normal and glaucomatous images. Automated glaucoma detection was created by employing structural and non-structural characteristics [23]. Automatic glaucoma diagnosis was created by [24] using segmentation of the optic disc and texture feature extraction. Pre-perimetric glaucoma detection with automated perimetry employing a DL classifier was described in [25]. An automated system for glaucoma identification using fundus pictures has recently been established [10]. The developed framework combines CNN with the generalized loss function and color-correcting algorithm to improve the results of the fundus photographic technique.

The basic CNN model that was used to train the network demonstrated how straightforward it was in comparison to more complex CNNs like Google LeNet and ResNet152. They proposed an automated glaucoma detection framework using a deep CNN retinex with color correction algorithm. This is done by utilizing hyper parameters pooling on the Region of Interests (ROIs) from retinex with a new loss function. The proposed method also uses a statistical test to preprocess the dataset.

1.1. Strengths

The Pipeline adjusts for illumination and color shifts prior to learning using Retinex-based normalization and colour balancing before performing ROI extraction and pooling; as such, it generates cleaner inputs and fixed-shape regions for the CNN that are free from acquisition artifacts and that enhance separability. Ablations reveal that allowing RO I and Retinex (Policy 4) consistently produces the best performance (e.g., Sensitivity ≈0.95-0.97, Specificity ≈0.99, Accuracy ≈0.97-0.99). It also achieves superior performance over published baselines in terms of recall, Precision, Accuracy and mAP@0.75 (Table 5), illustrating an external relative strength. Factor selections and the final model are additionally supported by statistical analysis (effect sizes, T-and P-values).

1.2. Limitations

The work also addresses that, albeit with limited availability, datasets are generally small and standardized benchmarking is lacking, limiting generalisability and comparability between studies and this, in turn, drives the research to wider multi-centre validation. While authors have shown that Retinex and colour correction alleviate lighting artifacts, the performance under extreme noise or blur is an open question outside of the preprocessing assumptions. Last, although ablation maps detail high gains using ROI/Retinex, further device diversity and prospective clinical testing would provide further assurance of robustness for in-situ deployments.

Novelties of the proposed model rely on removing coloring effects or noises generated from scanning devices, and then the prediction was performed over the image. Novelty is shown in various tables and figures in the remaining parts of this work, which are structured in the following manner. A related work that has been expanded upon can be found in Section II. In Section III, the proposed work is presented, which combines Retinex theory with a color correction algorithm based on CNN to determine the ideal values for the hyperparameters. In Section IV, results and discussion are presented, which show how well the associated performance worked out. The conclusion and the summary are presented in Section V.

2. Related Work

This section will offer a complete review of the present approaches, which will serve as the basis for discussing the following planned work. Deep learning, often known as deep neural networks, is a multi-layered Application of ANN. Deep neural networks are another common synonym for deep learning. In the last several decades, it has earned a reputation as one of the most successful tools. It has gained universal recognition in the academic community due to its ability to handle vast amounts of data. The fact that it can handle so much information is a major factor in this. The use of deeper hidden layers has been more popular in recent years because of their superior performance over more conventional methods in several areas, such as pattern recognition. CNNs are increasingly popular deep neural networks. Mathematically speaking, a "convolution" is a linear operation carried out between two matrices, and this is where the term gets its name.

CNN is comprised of the following four layers: Fully-connected Layer, Pooling layer, Non-linearity layer, and Convolutional Layer. Pooling and non-linearity layers are parameter-free, unlike convolutional and fully-connected layers. CNN layers are often necessary for training tiny feature detectors based on randomly picked picture patches. Calculating an image feature at a specific location is possible if the feature detector is convolved with the image at the location where the calculation is to be done [2]. Convolutional neural networks are unrivalled when it comes to processing audio, video, and speech data. The most significant are the Convolutional, Pooling, and Fully-Connected (FC) layers.

The work presented by [10] is an automatic DR classification system using CNN models with transfer learning, achieving 97.72% accuracy on the Kaggle dataset and 97.58% accuracy on the MESSIDOR dataset. It is usual practice to utilize a convolutional layer as the first layer in a convolutional network [27]. The initial Layer of a NN is always a convolutional layer. There may be more convolutional layers or pooling layers after these convolutional layers, but the fully connected Layer is always the very last Layer. Adding more layers to a CNN increases its complexity, hence its ability to recognize more and more of a picture. More complex features are highlighted at later stages, whereas basic ones like colors and borders are emphasized in the beginning. First, the network starts to identify the object's primary components or shapes as it processes the picture input via the CNN's layers, and then it continues to do so until it recognizes the item for which it was trained.

The convolutional Layer is the brain of a CNN and is responsible for the bulk of the network's processing. The term "invisible layer" is often used to describe this one. Data, a filter, and a feature map are required for successful operation. Here are the components. First, let's suppose the input is a colour photo with a three-dimensional pixel matrix. Therefore, the input will have three dimensions, one for each of the object's height, width, and depth in a two-dimensional picture. A height, breadth, and depth will be provided. They also use a feature detector, which traverses the image's receptive fields like a kernel or a filter to ascertain whether or not the feature is there. In this way, they can determine whether the feature exists. The formal term for this process is convolution [28].

The two-dimensional weighted array is used to construct the feature detector. This array will represent a segment of the picture. The receptive field could be any shape other than a standard three-by-three matrix, depending on the filter size. The larger the aperture of the filter, the larger the receiving field. After the filter is applied to a specific area of the picture, a dot product is used to find the connection between the input pixels and the filter [6]. An output array is then used to record the outcomes of the dot product computation. Once the kernel has covered the whole image, the filter will move forward one step, and the process will continue. Feature maps, activation maps, or convolved features are terms that describe the final result of many dot products taken from the input and the applied filter. After each convolution operation, a CNN incorporates non-linearity into its model by applying a Rectified Linear Unit (ReLU) to the feature map. The end result is a more intricate model.

2.1. Pooling Layer

Dimensionality Reduction By Pooling Layers. Another dimensionality reduction tool is pooling layers, sometimes called down-sampling. Using this strategy, we are able to reduce the overall number of parameters required. Like the convolution layer, the pooling operation takes a filter passed over the entire input, but the filter has no weights [28]. When in use, this filter is reminiscent of a convolutional layer. As a replacement, the kernel performs an aggregation function on the receptive field information to generate the output array. This means that the input array is not used directly by the kernel. As a concept, pooling may be broken down into two distinct types. It does this by repeatedly sliding the filter (max pooling) over the input, and selecting a pixel with the maximum value to pass to an output array. This process is called "travelling across the input" in computing jargon. This takes place as the process advances across the input. As an aside, this procedure is used more often than the technique of average pooling. Keeping this in mind, they shall proceed to the next statement. The filer moves over the input, calculates the average value within the receptive area and outputs it to the output array. The author can then further process this value. This is referred to as average pooling.

2.2. Fully-Connected Layer

The Layer's name, which is entirely related to all other layers, accurately describes the Layer itself. As mentioned above, the input picture's pixel values do not directly correlate with the output layer's values for pictures with only minimal connections between their layers. On the other hand, a fully linked output layer has direct connections between every node in the Layer below it. And so it is with the completely linked Layer.

This Layer is responsible for carrying out the classification process by using the attributes gathered from the previous layers and the filters that were unique to each of those layers. FC layers often utilize a softmax activation function, which provides a probability range of 0 to 1, to correctly classify inputs instead of the inclination [2]. DM as USD Deep learning has manifested strongly in both glaucoma diagnosis input modalities, fundus and OCT (sens/spec: 0.92/0.93 and 0.90/ 0.87; AUROC 0.90 and 0.86), though progression prediction is less strong and requires multimodal real-world validation [32]. A PRISMA-ScR bibliometric map of 3,581 articles reveals accelerating ML activity in fundus imaging and risk factors; momentum towards multimodal fusion and LLM-supported workflows [33]. Focused reviews report ≈93% diagnostic ac-

curacy but underpin the need for data diversity, standardization and explainability toward the clinical adoption [36]. In addition to images, the ERG-based SVM/CNN pipelines may facilitate signal-level detection, awaiting rigorous cross-device validation [35].

Nationwide screening analysis from Kazakhstan shows that tonometry-based programs are predominant, the incidence has increased, and there are cost/inequity concerns with potential to drive protocol and funding reforms [36]. Features such as OCT/OCTA/MRI derived with AI are facilitating better structural–vascular evaluations, but require reproducible cross-platform benchmarks [37]. Vision-language models (GPT-4V) demonstrate consistent feature-grading but are behind experts overall, indicating adjunct, not independent use until fine-tuned and for calibrated outputs [38]. Manually examining the optic nerve head is subjective, expensive, time-consuming, and varies with the examiner's skill, making it difficult to scale up for screening. Most automated ML pipelines on fundus images are unreliable and are often used as a black box predictor that cannot explain to the clinician or the patients how its predictions are being made, leading to a poor confidence in its use and acceptance.

Furthermore, existing methods (including recent work on SPL) often neglect acquisition-dependent illumination and color variations, which compromise separability of early signs; our ablations demonstrate that our model degrades significantly without Retinex and ROI (Policies 1–2 vs. Policy 4) in sensitivity, specificity and Accuracy, as this is a general fragility across existing pipelines. Last, noisy or saturated real-world images even degrade robustness, but explicit colour correction/Retinex contributes to recovering informative structure. These deficiencies drive our pre-CNN normalization, followed by ROI design and the relative experiments, which are accordingly shown in this paper.

3. Proposed Work

In this project, they use DL to solve the problem of glaucoma detection. In previous research, a low-level CNN was combined with the retinex algorithm and statistical tests, which caused more false positives and prevented the detection of glaucoma in its early stages. Since there was a need for a solution to this problem, they introduced a colour correction algorithm with retinex that handled the colour differences between the earlier and later stages of the disease. Figure 1 provides the architecture of the proposed work. Initially, the datasets pass into the preprocessing section, where images are filtered and augmented, then into the retinex section, which removes artificial parts from images and makes them original. This artificial part is the saturation and contrast that the image-capturing device adds. After cleaning the image region of interest, the irregularity-removed images are passed into the deep convolutional neural network to perform detection over images with defined parameters and return whether the image contains glaucoma.

The proposed work's high-level overview is defined in Figure 1, which not only shows the place for the modeling in the Pipeline but also explains the way the dataset moves in the complete system, as it is observable that the dataset is filtered out in the initial stages so that color correction algorithm works upon it which makes feature extraction faster and more detailed features were extracted on these features resting is performed and images were converted into constant sizes then passed into convolution which predicts regions were glaucoma resides in the scans.

Figure 2 provides a visual representation of the basic structure of the suggested method. This is comprised of three primary components. Part 1 and Part 3 will be discussed first. The findings of Part 1 indicate that 899 out of a total of 1450 fundus pictures had glaucomatous signs. The Taiwanese hospital Kaohsiung Chang Gung Memorial (KCGM) was responsible for the donation of 551 organs, all of which were in outstanding condition. The proportional proportions of each set used for training, validation, and testing were fifty percent (20%), twenty percent (30%), and thirty percent (30%).

Samples were preprocessed with transformations and the decoloring algorithm to enhance the region of glaucoma in the image. This makes the modeling process simple and generates good results over unknown image samples. The efficiency of the proposed model not only relies on CNN, as the model Pipeline itself was trained in a manner that is not able to effectively reduce overhead during training, but also in preprocessing steps, as without the proper required data input, model performance will not be decided,the proposed model effectively packed with color correction, and CNN in which CNN is working upon the features defined over corrected colored images by coloring algorithm.

3.1. Block, Epoch, and Batch

They will begin by investigating the link between epochs and blocks. The system's intended architecture consists of a total of l blocks, where $l = 10$ blocks. Because the benchmark for the training, validation and test sets is always the same within each Block, the term "block" refers to Block i, which has h_i epochs, where $h_i <= h$ and $i = 1, 2, \ldots l$. It was determined that $h = 50$ is the maximum number of epochs per Block. H_i will equal h if the termination rule was not met. 50% of the sample were able to capture all the different variations for glaucoma shown scans, and adding more samples makes it lead to bias towards a particular pattern, and results might be altered, as reducing samples by 50% leads to missing some of the important behavior of the dataset, which makes it difficult to decide on taking 50% of the samples for training. Figure 2, part 3, demonstrates the process of building a block model, which the test set will be utilized to output performance statistics at the end of the final epoch of each Block. They then explored the interplay between epochs and batches. Each epoch contained b = 40 batches with m = 40 images in each batch.

We employed the nearby Block's training set to randomly select each one of the m = 40 images in the batch. Every picture in each batch was processed using a pre-CNN technique (Step 0-4 in CNN, Step 5-8 in Figure 4). Using the amended data, a prevalidation model was created. Pre-CNN processing and CNN processing on picture collections. A channel represents the Colors, and the block size was configured based on the coloring algorithm, which avoids making the color intensity of the pixel constant as in the original images. If a block were not manipulated, then due to the coloring algorithm, actual intensity values may get changed, and information may be altered from the original format. Figure 3 depicts the preliminary CNN procedure. The sizes of the image are scaled by using common scaling and transformation exercises. 2 strides of size 3X5 were used to scale the image to the desired results, and similarity padding was added to compare. Figure 4 illustrates the CNN process phases. Block refers to the mini-batches and epochs defined as one round from input to output and reserve back from output to the input node. This complete state is called as one epoch.

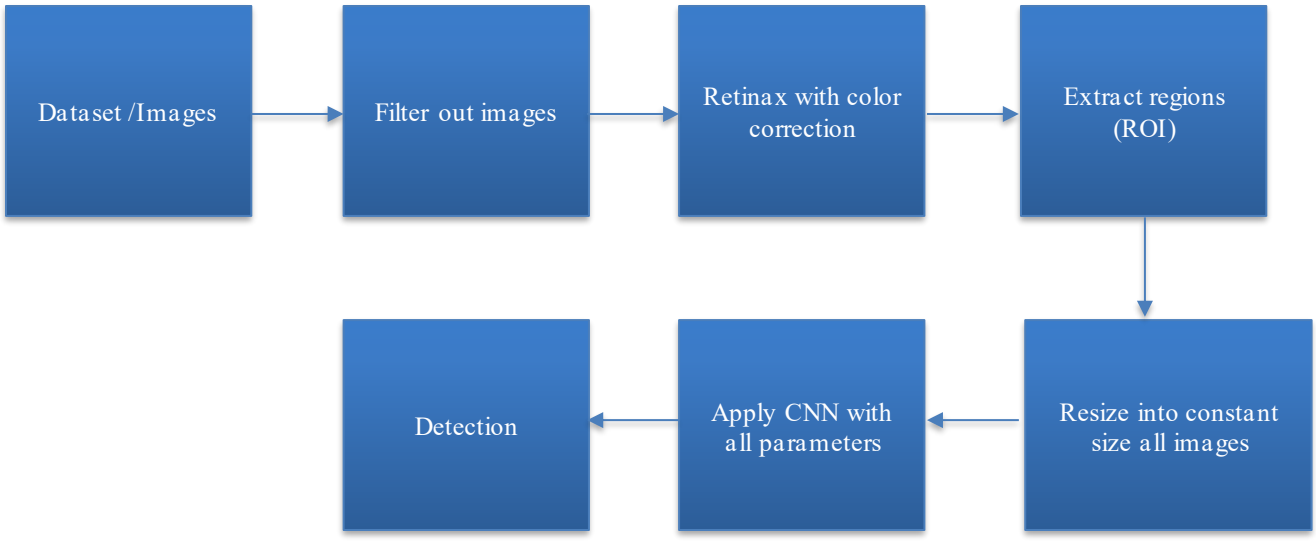

Fig. 1 Workflow of proposed model

3.2. Pre-CNN Process

This section presents an overview of the pre-CNN approach, which may be summarized as Steps 0 through 4, as seen in Figure 3. The numbers after "input and output" indicated the total number of images in proportion to their R, G, and B values. Figure 3 @500*700 corresponds to the number of row and column pixels, respectively. The number 0 in indicates three R-G-B pictures, each of which has 00 row pixels and 70 column pixels, respectively.

Following is the detailed explanation of Steps 0 through 4, starting with the first:- The term "cortex" was merged with "retina" to produce. The eye's retina is responsible for color perception, and the cortex is the brain region that processes the information it receives from the retina. Together, these two ingredients comprise the phrase "retinex". Images that are clean have had all of their text replaced with pixel 0, which is equivalent to the colour black. A variety of augmentations are added. Finally, the statistical test is done to determine ROI.

3.3. Mathematical and Statistical Calculations Over Images to Make and Test Hypothesis

The proposed generalized cross-focal entropy will be employed as the loss function, denoted by L, for each picture that is included in the trainset [22, 10].

Algorithm 1: Proposed Pre-CNN Algorithm

```
Input:raw image data set.
Output:preprocessed data set.
1:Foreach I in range(shape.dataset):
2:I←I.cv.rotate().
3:I←I.cv.horizontalScale().
4:I←I.cv.Remove_Blurr().
5:Return I.
```

Algorithm 1 performs data preprocessing tasks, as datasets of images may have low variance and noise in them. To handle such cases of datasets, this algorithm performs rotation over images, which generates the same number of images after the rotation.

Then, it performs horizontal scaling on the images, which gives a different variety of data to the training set. Some images may also contain blurry noise in pixels, creating a hassle for the algorithm in the learning process.

Then the algorithm returns images, and now the dataset has also increased in size as more samples of the same images are available.

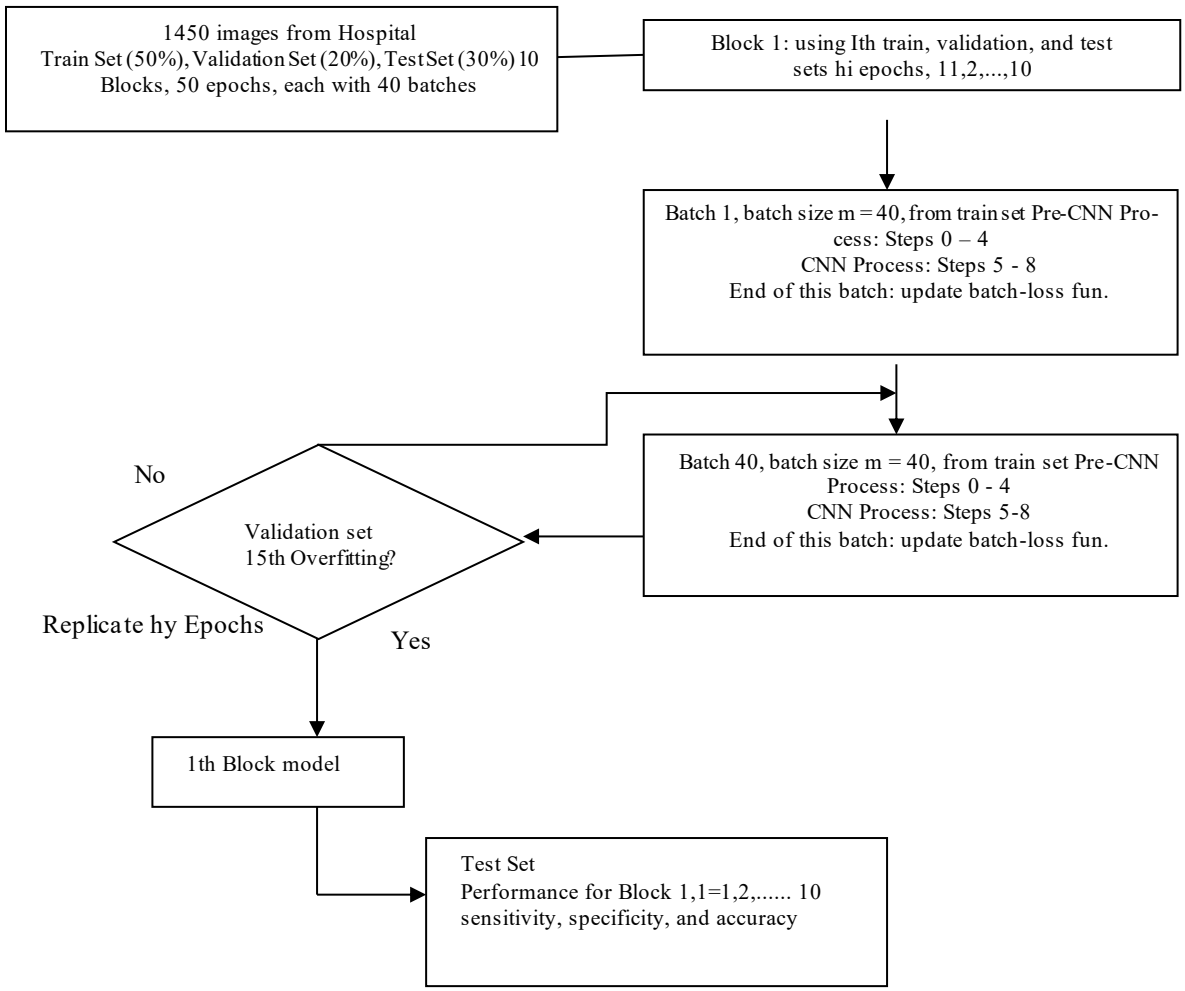

Fig. 2 Framework of proposed model

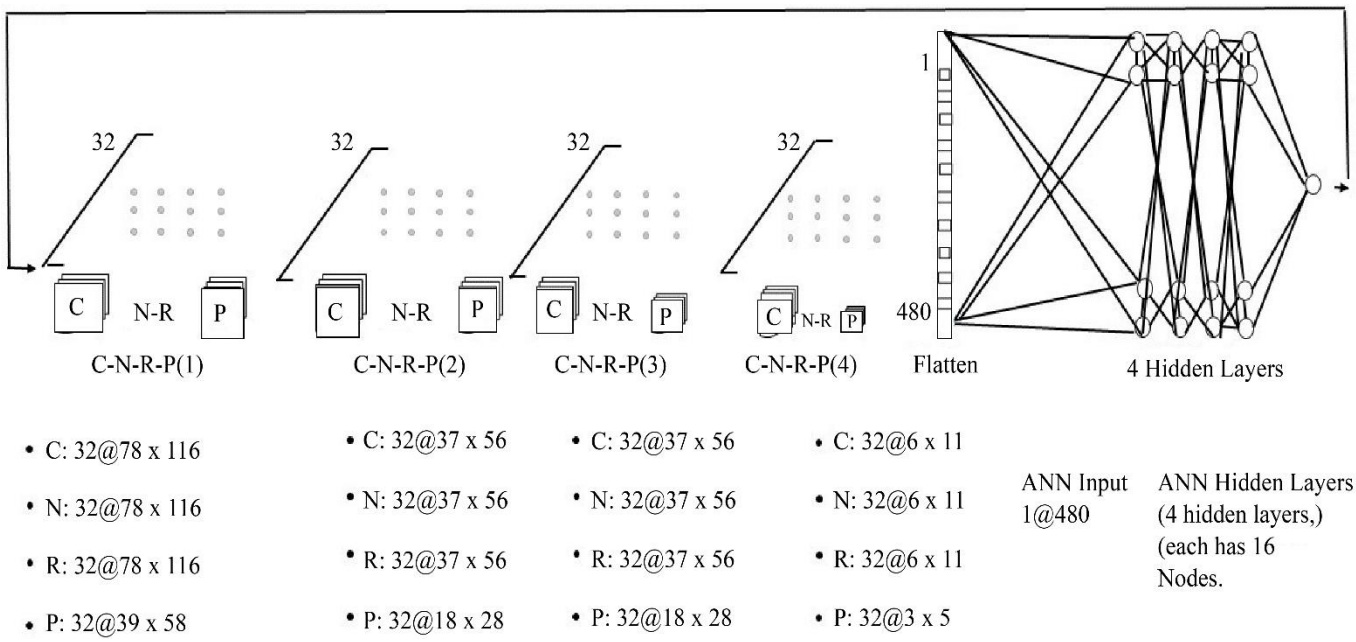

Fig. 3 Framework of a pre-CNN model

$$L_{\text{fun}}(\hat{y}\, i, yi) = -(1/m)\sum_{i=1}^{m}(yi \log \hat{y}\, i + (1-y_i)\log(1-\hat{y}_i)) \quad (1)$$

Where y_i refers to the true label, $\hat{y}_1$ is the predicted

Results for the Class $y_i = 1$;

$$L_{fun}(\hat{y}_i, y_i) = -(1/m)\sum_{i=1}^{m}(y_i \log \hat{y}_i) \quad (2)$$

$$L_{fun}(y_i, y_i^p) = \sum_{i=1}^{m} (\log(\cos h(y_i^p - y_i))) \quad (3)$$

Upon the introduction of a focusing parameter γ.

The contribution of simple samples will diminish as the concentration of the parameter increases. To further address the problem of class imbalance, the idea of attention loss has included a weighting component represented by the symbol. Consequently, the definition of focus loss may be articulated in an alternative manner as:

$$L_{fun}(y_i, y_i^p) = \sum_{i=y_i<y_i^p}^{m}((\gamma - 1).|y_i - y_i^p|) + \sum_{i=y_i>=y_i^p}((\gamma).|y_i - y_i^p|) \quad (4)$$

3.4. CNN Process

Determining the parameters and hyperparameters inherent to the methodology is the first step in developing a data transformation and classification strategy.

In using CNN specifically, among the first and most important steps is to set hyperparameter values (e.g., specific values for each convolution layer, number of hidden layers, and number of nodes within each hidden Layer) and parameter values (e.g., weights at each hidden Layer) for modeling.

CNN surpasses all their models in detection tasks, Specifically associated medical imaging as images contain noises and specific colored patil space images, in order to extract features from the spatial images, CNN performs extraction and prediction with higher Accuracy, which makes using CNN in this particular case.

When time complexities are taken into consideration, the proposed model outperforms existing ones as editing solutions perform various operations like contrast stretching and histogram equalization to enhance images, which adds time overheads, but in the proposed color correction step, it reduces this overhead and makes it better in terms of time complexities as well. Below, you will find the hyperparameter values and a detailed explanation of the rules that were actually used. Predetermined hyperparameters include the following:

1. Kernel matrix:3 *3
2. The complete number of blocks is ten
3. The complete quantity of epochs is fifty
4. The overall sum of batches is forty
5. The number of batches: forty
6. The rule for terminating the replication for an epoch states that it must be stopped if it has been overwritten more than 15 times.

Algorithm 2: Proposed CNN Algorithm
Input: image dataset.
Output: constant regions.
1: The dataset batch was created as D1, D2, and D3.Dn
2: For each dataset batch D:
3: Preprocess every image I in D.
4: OpenCV2.Get_color_cord(I) ← CmI.
5 : CmI ← R3(CmI).
6: For each CmI:
7: Exp(−((CmI)/2x3)2) → ROI.
8 : For each ROI :
9: ROI → ROI X 3X3 → ROIC

The proposed CNN models described in Algorithm 2 begin with batching the dataset into the data batch splits. These splits are preprocessed by image processing steps, which remove noisy images, determine the size of the test, train and then augment images. Furthermore, these processed images are passed into openCV and get the color cord function. Thus, it returns the coordinates of color values and matches these coordinates with the Histogram of all images to perform color matching. Using Equation 1 removes the artificial light or blurriness, and create images in their original form. Thereafter, regions from the images are extracted and stored in the ROI array. Part of the Pipeline runs as a background process, as each region was visualized in every iteration to reduce the overheads, and a single image containing various regions that are segmented and further processing was performed to avoid visualizing overheads. After that, it performs pooling over these regions at the end to return objects in constant shapes from the regions, which are ready to pass into a deep convolutional neural network to detect whether that particular frame is glaucoma or not. In the last or output Layer, the softmax function was used to predict whether a particular scan was affected or not by glaucoma.

Figure 4 describes the steps of the proposed CNN model. By utilizing low-cost colour fundus photography as the mainstream approach, the approach is brought closer to population-level screening as well as tele-ophthalmology, especially in resource-constrained environments. Second, the Pipeline is now more resilient to scanner variability and demographic variability, incorporating both luminance and colour normalization in a Retinex framework, which specifically compensates for scanner-induced artefacts; such robust performance is needed not only for mixed fleets of cameras in clinical deployment.

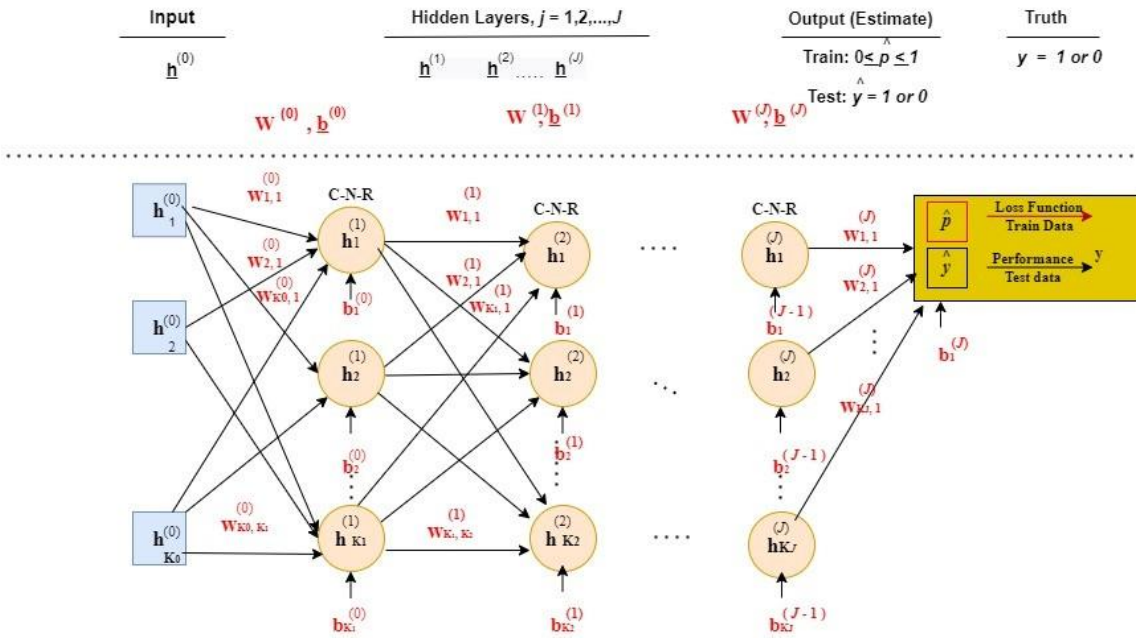

Fig. 4 Framework of proposed CNN model

The ROI, Retinex-based ablation (Policy 4) performs extremely well in terms of sensitivity/specificity/accuracy (≈0.95–0.99), suggesting the device can serve as a first-pass triage tool and help avoid cases that would be missed as false negatives or costly false positives. Complementary results in head-to-head comparison (Recall 96.6%, Precision 97.5%, Accuracy 98.3%, mAP@0 75 97.9%) also reflect clinical reliability. This research further notes the immediate application relevance to screening workflows, while also recognizing the need for broader validation across multiple centres, given the historically modest and heterogeneous datasets used in glaucoma research (1,450 images; 899 glaucomatous; KCGM subset n=551; defined train/val/test splits).

3.5. Statistical Tests

This research quantified factor effects on mean performance using effect sizes, coefficients, T-values, and P-values (Table 1). Factors included image size (A), convolution layers (B), number of kernels (C), hidden layers (D), number of nodes (E), a preprocessing toggle (F), and loss parameters (G). Several factors (e.g., convolution layers) showed statistically significant influence with large |T| and small P, guiding the final hyper-parameter choices. Experiments followed a fixed design of 10 blocks, each with up to 50 epochs, 40 batches/epoch, batch size = 40, with an early-stop rule if overfitting recurred >15 times; sensitivity, specificity, and Accuracy were computed per Block and summarized across ablations.

3.6. Retinex Integration

Retinex-based illumination normalization plus color correction is applied before ROI selection and CNN to remove device-induced saturation/contrast artifacts and restore original chromaticity. Implementation uses OpenCV color-coordinate extraction and histogram matching; the correction step explicitly "removes the artificial light or blurriness," yielding cleaner inputs for feature learning. Ablations confirm its value: policies enabling Retinex and ROI deliver the highest sensitivity/specificity/accuracy, and Table 4 attributes the significant improvements to appending color correction with Retinex.

4. Experimental Results

In this part, they will examine the advantages of the proposed method over the alternatives already in use. First, they determine the effect size and the associated P-value for the mean response. In addition, the efficiency of different loss functions for insurance plans like ROI* and Retinex. The mean performance and related standard error (a*) are then calculated for the four Policies (ten blocks, two replications, convolutional neural network, suggested loss function: a=1, =1.5). The recommended strategy and the most recent methodology are used in these computations. The best results and their standard errors (a*) for the four policies are then obtained using 10 Blocks, 2 Replications, and CNN with the recommended loss functions (A=1,=1.5).

4.1. Dataset Description

For the REFUGE (Retinal Fundus Glaucoma Challenge) dataset hosted on Grand Challenge, the corpus contains 1,200 color fundus photographs, split evenly into 400 training, 400 validation, and 400 test images. Refuge. Grand-challenge orgNature Images were captured on two devices—training on Zeiss Visucam 500 (≈2124×2056 px) and validation/test on

Canon CR-2 (≈1634×1634 px)—to introduce device variability. Nature Class balance is stratified at roughly 10% glaucomatous (≈120) and 90% non-glaucomatous (≈1080) across splits. PMCResearchGate Regarding demographics, published descriptions indicate the images are from Chinese subjects, but age/sex breakdowns are not provided in the public release materials.

Glaucoma is one of the most prevalent eye illnesses worldwide and one of the main preventable causes of permanent blindness in working-age adults. It employed Colour Fundus Photography (CFP), which has the lowest overall cost compared to other imaging modalities, to check for retinal abnormalities.

So far, its only contribution to glaucoma research has been computing a few associated biomarkers. The vertical cup-to-disc ratio is one illustration of this. This is the outcome that directly results from the restrictions the strategy imposes. Despite their broad usage in medical image analysis, deep learning algorithms have not been significantly used in evaluating glaucoma due to the limited quantity of data presently accessible.

This is because the presently accessible data sets are quite modest in size. Additionally, it is challenging to evaluate different processes in a way that is consistent throughout since there is no standardized benchmarking methodology in place. To find solutions to these problems, they established the Retinal Fundus Glaucoma Challenge, often known as REFUGE (https://refuge.grand-challenge.org).

In connection with the MICCAI 2018 conference, the challenge was organized. The difficulty could be broken down into two main parts: the first was classifying glaucoma, and the second was separating the optic disc and cup. These two elements were equally difficult. As a part of the REFUGE project, they have made a data set including 1200 fundus images, ground truth segmentations, and clinical glaucoma labels available to the general public. This collection of data was produced. This data collection is available at the most extensive time [29]. In addition, they have built an evaluation methodology to allow and ensure fairness in the comparison of varied models, which would hopefully encourage the development of innovative methods within the domain-a total of 12 teams qualified to compete in the online challenge.

This study provides a synopsis of their research procedures and an analysis of the associated findings. In particular, they found that two of the teams that finished in first place performed better than two human specialists when it came to classifying glaucoma cases. In addition, the results of the segmentation were, for the most part, comparable with the ground truth annotations. Furthermore, the results produced complementary outcomes that can be utilized to a greater extent by assembling the findings.

4.2. Performance Evaluation

4.2.1. Sensitivity/Specificity

To compute the sensitivity and specificity of the RULES configuration that is being investigated using an assessment methodology developed from an earlier article that was published [31], and according to the formulae listed below:

$$Sensitivity = TP/(TP+FN) \quad (5)$$

$$Specificity = TN/(TN+FP) \quad (6)$$

4.2.2. Accuracy

The metric has been extensively used in assessing the efficacy of binary classification systems, with the Area Under the Curve (AUC) value, corresponding to the area under the receiver operating characteristic curve, ranging from 0 to 1. The fact that the AUC value is so high is evidence of the excellent performance of the classifier [11].

$$\text{Accuracy} = \frac{TP + TN}{TP + TN + FP + FN} \quad (7)$$

The values successfully predicted are denoted by True Positive (TP) and True Negative (TN), respectively. On the other hand, False Positives (FP) and False Negatives (FN) are examples of events that were misclassified.

4.3. Results and Discussion

This sub-section explores and compares four different strategies in terms of sensitivity, specificity and Accuracy. Policies were given for the entire cross-section range, from Policy 1, which applied neither ROI nor retinex, to Policy 4, which applied both retinex and ROI. Policies were provided for all cross-sections.

Below is a summary of the results displayed in the tables.

1. Table 5 shows various hypotheses testing values in the proposed model and in the existing solution. How it changes in experiments makes the proposed models work better than the existing solution in every parameter efficiency. This is because of the introduction of deep hidden layers of 128 layers, which reduces the effects of parameters.
2. Table 2 compares sensitivity, specificity and Accuracy values of proposed and existing solutions, which show that the proposed solutions significantly produce better results due to color correction in the initial steps, which makes the decision boundary more separable and the detection task easier for the model to detect glaucoma in it.
3. Table 3 compares performance on different loss functions, and it shows that adding pooling layers makes functions to reduce the number of false positives and improve the values of sensitivity, specificity, and Accuracy on all parameters, even though ROI and retinex are absent in experiments, it also produces better results.

4. Table 4 explains that appending color correction with retinex makes images more noise-free and reduces cases, which increases bias in detection tasks, which makes specificity, sensitivity, and Accuracy better than existing solutions with significant improvements.

4.3.1. Illustrative Example

Figure 5 represents a preview of the dataset images, then shows actual images of glaucoma and presents eye scans.

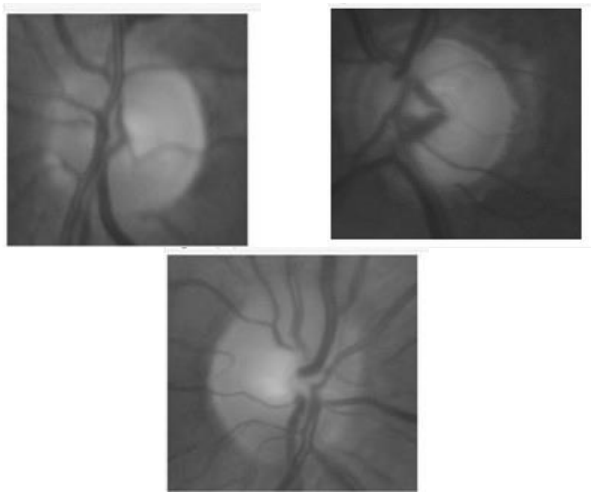

Fig. 5 Dataset Images and Actual Images of Glaucoma

Figure 6 shows that the coloring algorithm makes images saturated, which makes the algorithm extract important features easily and find regions of interest faster than the original images.

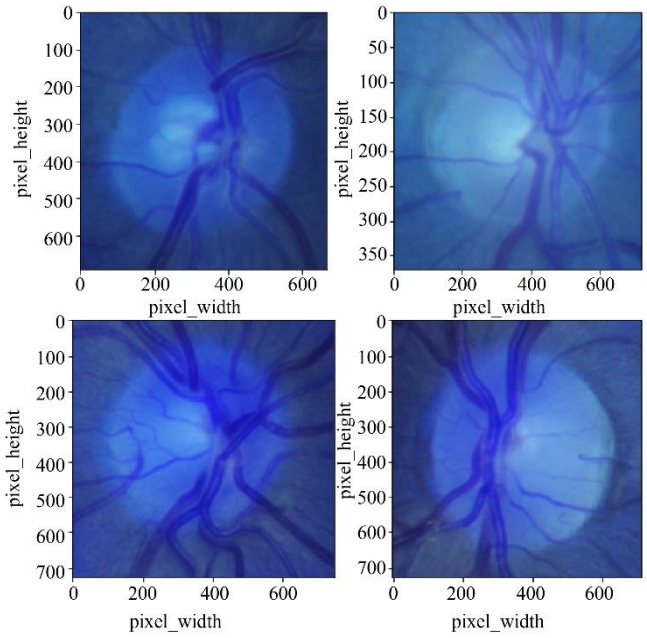

Fig. 6 Images using the coloring algorithm

4.3.2. Tensorboard Graphs

Figures 7, and 8 show the graph of the relationship between decreasing loss values with respect to epochs during training. In each loss curve, the X-axis represents epochs and the Y-axis represents particular losses. Optimization for layer-level Adam was used. For handling overfitting, Dropout layers were taken into consideration. To make the gradients converge at the best point, learning rates were passed into a set of [0.01,0.15,0.1] from which 0.15 gives higher scores and d considered for the final Pipeline.

- Loss curve: The loss values are consistently decreasing, indicating that the model obtains its optimum weight values until the last backwards propagation.
- Accuracy per epoch: The Below curve shows that even though Val and train loss find global values for weights, each region also has their own local optimum values for weights in each epoch, which causes fluctuations in Accuracy per epoch.

4.3.3. Model Graphs

Figure 9 shows the graphical representation of the model trained with transferred learning of existing and building new pipelines with add-on tasks.

4.3.4. Comparison Result

Table 5 shows the comparison analysis of performance metrics for the glaucoma detection models. The models chosen for comparison are vested in class for detection purposes.

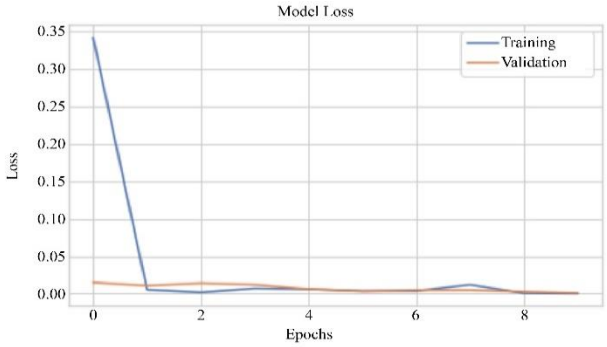

Fig. 7 Loss curve

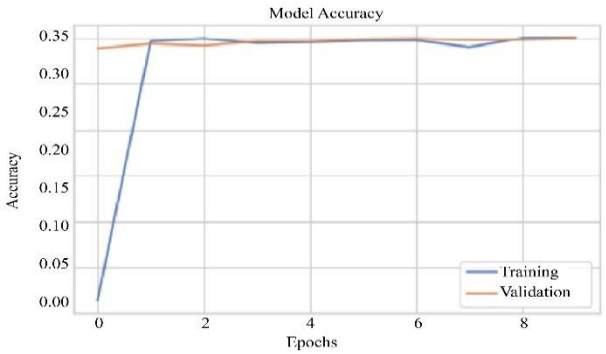

Fig. 8 Accuracy per epoch

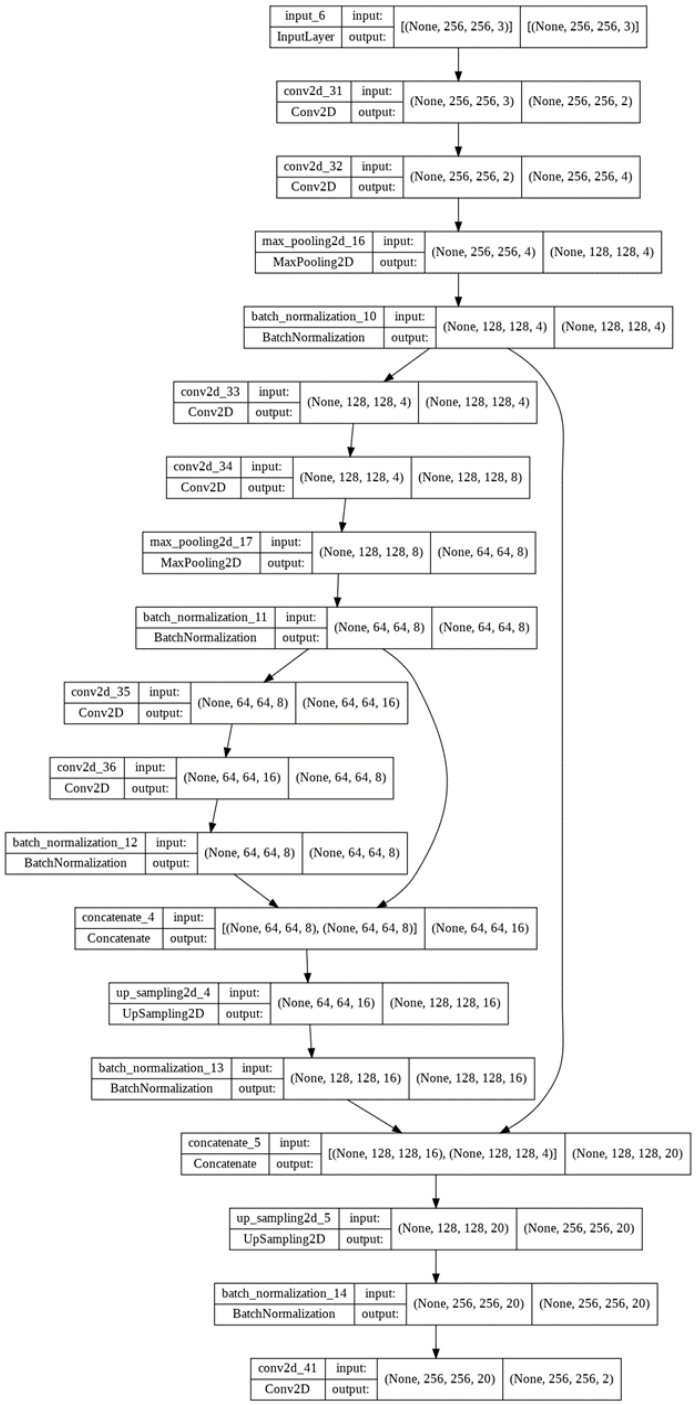

Fig. 9 Model evaluation

The proposed model surpasses the performance, generates a score that shows significant improvement over the benchmarking models, and generates results even on images with noisy pixels. Across five published baselines, performance spans Recall 56.4–74.9%, Precision 60.0–73.4%, Accuracy 65.3–69.8%, and mAP@0.75 78.0–88.0%. The Proposed model markedly exceeds these ranges, achieving 96.6% Recall, 97.5% Precision, 98.3% Accuracy, and 97.9% mAP@0.75. Versus the best prior results, absolute gains are +21.7 pp Recall (96.6 vs 74.9), +24.1 pp Precision (97.5 vs 73.4), +28.5 pp Accuracy (98.3 vs 69.8), and +9.9 pp mAP@0.75 (97.9 vs 88.0). Relative to the average baseline, improvements are similarly large: +31.06 pp Recall, +30.38 pp Precision, +30.5 pp Accuracy, and +15.06 pp mAP@0.75.

These margins indicate stronger detection and better calibration at stricter IoU (0.75), supporting the method's robustness and practical screening value.

Table 1. Effect and P-values W.R.T. mean response

		Effect	Proposed Effect	Coefficient	Proposed Coefficient	T-value	Proposed T-value	P-Value	Proposed P-value
A	(Image size)	-0.0313	-0.00012	-0.0156	0.000034	-1.06	0.01	0.303	0.19
B	(Conv.Layers)	-0.1313	0.001	-0.0657	0.02	-4.47	0.0007	0	0
C	(no.Kernel)	0.0178	0.00034	0.0089	0.01	0.6	0.11	0.554	0.21
D	(HiddenLayers)	-0.0776	0.00051	-0.0388	0.0013	-2.64	1.91	0.018	0.00096
E	(no.nodes)	-0.0028	-0.0001	-0.0014	0.00051	-0.09	0.00089	0.926	0.164
F	(dclctcorfill)	-0.1316	0.00008	-0.0657	0.00001	-4.48	0.0041	0	0
G	(ParaA,binloss	-0.0706	0.01231	-0.0353	0.0012	-2.4	0.00061	0.029	0.00012

Table 2. Performance among various loss functions for policy (Roi* + Retinex)

Loss Function	Mean (9*)					
	Sensitivity	Proposed Sensitivity	Specificity	Proposed Specificity	Accuracy	Proposed Accuracy
Proposed (a=1,b=1.5)	0.95(0.03)	0.98(0.01)	0.98(0.03)	0.99(0.03)	0.97(0.01)	0.99(0.03)
Foca lLoss (a=1,b=1)	0.93(0.05)	0.99(0.03)	0.92(0.05)	0.95(0.02)	0.92(0.04)	0.96(0.05)
Cross Entropy (a=1,b=1)	0.91(0.03)	0.95(0.01)	0.93(0.05)	0.97(0.01)	0.92(0.03)	0.99(0.03)
MSE	0.92(0.03)	0.97(0.03)	0.93(0.05)	0.98(0.03)	0.93(0.03)	0.99(0.03)

Table 3. Mean performance and its standard error (A*) for the four policies: 10 blocks, 2 replications, CNN with the proposed loss function (A=1,=1.5)

Policy	ROI*	Retinex	Mean (a*)					
			Sensitivity	Proposed Sensitivity	Specificity	Proposed Specificity	Accuracy	Proposed Accuracy
1	NO	NO	0.72(0.13)	0.83(0.03)	0.63(0.23)	0.70(0.03)	0.69(0.21)	0.79(0.20)
2	YES	NO	0.80(0.12)	0.89(0.32)	0.72(0.13)	0.79(0.03)	0.78(0.13)	0.83(0.23)
3	NO	YES	0.90(0.04)	0.98(0.14)	0.96(0.05)	0.99(0.15)	0.91(0.05)	0.97(0.15)
4	YES	YES	0.95(0.03)	0.99(0.003)	0.98(0.03)	0.99(0.13)	0.97(0.01)	0.99(0.11)

Table 4. Optimal performance and its standard error (A*) for the four policies: 10 blocks, 2 replications, CNN with the proposed loss functions (A=1,= A=1.5)

Policy	ROI*	Retinex	Mean (a*)					
			Sensitivity	Proposed Sensitivity	Specificity	Proposed Specificity	Accuracy	Proposed Accuracy
1	NO	NO	0.92(0.1)	0.97(0.01)	0.73(0.11)	0.93(0.1)	0.77(0.1)	0.87(0.20)
2	YES	NO	0.90(0.1)	0.93(0.21)	0.69(0.1)	0.95(0.1)	0.80(0.1)	0.81(0.01)
3	NO	YES	0.97(0.04)	0.99(0.04)	0.99(0.15)	0.99(0.05)	0.97(0.05)	0.99(0.01)
4	YES	YES	0.97(0.03)	0.99(0.13)	0.99(0.03)	0.99(0.03)	0.98(0.01)	0.99(0.03)

Table 5. Comparing proposed method with existing algorithms

Model	Recall (%)	Precision (%)	Accuracy (%)	mAp75 (%)
De [3]	74.9	73.4	69.8	88
Li [8]	74.1	71.5	69.2	84.2
M.P. Karthikeyan [22]	63.3	64.2	66.2	83
Albawi [26]	56.4	60	65.3	78
Chen [2]	59	66.5	68.5	81
Proposed	96.6	97.5	98.3	97.9

5. Conclusion

In this work, they solve the problem of glaucoma detection using deep learning. In previous works, a low-level CNN is used with the retinex algorithm and statistical tests, resulting in false positives and an inability to detect glaucoma in its early stages because the colour of the scan in the earlier phase differs from that in the mature phase. This is why they introduced the colour correction algorithm with retinex, which handles the colour and male models to detect glaucoma even in its early stages. Another issue is that existing solutions generate false positives, which is wrong in terms of health issues. For example, if a person has died, then the model does not predict

it. These cases are dangerous in some scenarios, which is why there is a sudden need to reduce false positives by adding more hidden layers. The time taken for the modeling process is in the form of O(Log2NxN×2N), where classification tasks and preprocessing take the major chunks of the timelines and make the modeling heavier in terms of time.

Optimization was avoided in the preprocessing phase as it generates image pixels that create fake illusions in images, which affects the detection capability of the CNN models.

That is why only Adam is used for optimization on network layers and not in any preprocessing and post-processing sections. This work pipeline suits population screening and tele-ophthalmology, using low-cost fundus images with Retinex normalization to handle device variability. Clinically, it supports early-detection triage and referral prioritization. Future work includes multi-centre, cross-device validation with demographics, multimodal fusion with OCT, prospective deployment studies, and threshold calibration balancing sensitivity, specificity, and workload constraints.

References

[1] Kwokleung Chan et al., "Comparison of Machine Learning and Traditional Classifiers in Glaucoma Diagnosis," *IEEE Transactions on Biomedical Engineering*, vol. 49, no. 9, pp. 963-974, 2002. [CrossRef] [Google Scholar] [Publisher Link]

[2] Xiangyu Chen et al., "Glaucoma Detection Based on Deep Convolutional Neural Network," *2015 37th Annual International Conference of the IEEE Engineering in Medicine and Biology Society (EMBC)*, Milan, Italy, pp. 715-718, 2015. [CrossRef] [Google Scholar] [Publisher Link]

[3] Alan Carlos de Moura Lima et al., "Glaucoma Diagnosis Over Eye Fundus Image Through Deep Features," *2018 25th International Conference on Systems, Signals and Image Processing (IWSSIP),* Maribor, Slovenia, pp. 1-4, 2018. [CrossRef] [Google Scholar] [Publisher Link]

[4] Tehmina Khalil, Samina Khalid, and Adeel M. Syed, "Review of Machine Learning Techniques for Glaucoma Detection and Prediction," *2014 Science and Information Conference*, London, UK, pp. 438-442, 2014. [CrossRef] [Google Scholar] [Publisher Link]

[5] Seong Jae Kim, Kyong Jin Cho, and Sejong Oh, "Development of Machine Learning Models for Diagnosis of Glaucoma," *PLOS One*, vol. 12, no. 5, pp. 1-16, 2017. [CrossRef] [Google Scholar] [Publisher Link]

[6] Zheng Chengjie et al., "Artificial Intelligence in Glaucoma," *Current Opinion in Ophthalmology,* vol. 30, no. 2, pp. 97-103, 2018. [CrossRef] [Google Scholar] [Publisher Link]

[7] Zvia Burgansky-Eliash et al., "Optical Coherence Tomography Machine Learning Classifiers for Glaucoma Detection: A Preliminary Study," *Investigative Ophthalmology and Visual Science,* vol. 46, no. 11, pp. 4147-4152, 2005. [CrossRef] [Google Scholar] [Publisher Link]

[8] Fei Li et al., "Visual Field-Based Automatic Diagnosis of Glaucoma using Deep Convolutional Neural Network," *International Workshop on Ophthalmic Medical Image Analysis*, Granada, Spain, pp. 285-293, 2018. [CrossRef] [Google Scholar] [Publisher Link]

[9] Tanzila Saba et al., "Fundus Image Classification Methods for the Detection of Glaucoma: A Review," *Microscopy Research and Technique*, vol. 81, no. 10, pp. 1105-1121, 2018. [CrossRef] [Google Scholar] [Publisher Link]

[10] Wheyming Tina Song, Ing-Chou Lai, and Yi-Zhu Su, "A Statistical Robust Glaucoma Detection Framework Combining Retinex, CNN, and DOE using Fundus Images," *IEEE Access*, vol. 9, pp. 103772-103783, 2021. [CrossRef] [Google Scholar] [Publisher Link]

[11] Lauren J. Coan et al., "Automatic Detection of Glaucoma via Fundus Imaging and Artificial Intelligence: A Review," *Survey of Ophthalmology*, vol. 68, no. 1, pp. 17-41, 2022. [CrossRef] [Google Scholar] [Publisher Link]

[12] S. Sankar Ganesh et al., "A Novel Context-Aware Joint Segmentation and Classification Framework for Glaucoma Detection," *Computational and Mathematical Methods in Medicine*, vol. 2021, pp. 1-19, 2021. [CrossRef] [Google Scholar] [Publisher Link]

[13] Neeraj Gupta, Hitendra Garg, and Rohit Agarwal, "A Robust Framework for Glaucoma Detection using CLAHE and EfficientNet," *The Visual Computer International Journal of Computer Graphics*, vol. 38, no. 7, pp. 2315-2328, 2021. [CrossRef] [Google Scholar] [Publisher Link]

[14] Md. Sarwar Kamal et al., "Explainable AI for Glaucoma Prediction Analysis to Understand Risk Factors in Treatment Planning," *IEEE Transactions on Instrumentation and Measurement*, vol. 71, pp. 1-9, 2022. [CrossRef] [Google Scholar] [Publisher Link]

[15] José Ignacio Orlando et al., "Refuge Challenge: A Unified Framework for Evaluating Automated Methods for Glaucoma Assessment from Fundus Photographs," *Medical Image Analysis*, vol. 59, pp. 1-47, 2020. [CrossRef] [Google Scholar] [Publisher Link]

[16] Marriam Nawaz et al., "An Efficient Deep Learning Approach to Automatic Glaucoma Detection using Optic Disc and Optic Cup Localization," *Sensors*, vol. 22, no. 2, pp. 1-18, 2022. [CrossRef] [Google Scholar] [Publisher Link]

[17] Yasmeen George et al., "Attention-Guided 3D-CNN Framework for Glaucoma Detection and Structural-Functional Association using Volumetric Images," *IEEE Journal of Biomedical and Health Informatics*, vol. 24, no. 12, pp. 3421-3430, 2020. [CrossRef] [Google Scholar] [Publisher Link]

[18] Liu Li et al., "A Large-Scale Database and a CNN Model for Attention-Based Glaucoma Detection," *IEEE Transactions on Medical Imaging*, vol. 39, no. 2, pp. 413-424, 2019. [CrossRef] [Google Scholar] [Publisher Link]

[19] Liu Li et al., "Attention based Glaucoma Detection: A Large-Scale Database and CNN Model," *Proceedings of the IEEE/CVF Conference on Computer Vision and Pattern Recognition (CVPR),* Long Beach, CA, USA, pp. 10571-10580, 2019. [Publisher Link]

[20] Arunava Chakravarty, and Jayanthi Sivswamy, "A Deep Learning based Joint Segmentation and Classification Framework for Glaucoma Assessment in Retinal Color Fundus Images," *arXiv Preprint*, pp. 1-8, 2018. [CrossRef] [Google Scholar] [Publisher Link]

[21] Shubham Joshi et al., "Glaucoma Detection using Image Processing and Supervised Learning for Classification," *Journal of Healthcare Engineering,* vol. 2022, no. 1, pp. 1-12, 2022. [CrossRef] [Google Scholar] [Publisher Link]

[22] M.P. Karthikeyan, E.A. Mary Anita, and D. Mohana Geetha, "Towards Developing an Automated Technique for Glaucomatous Image Classification and Diagnosis (AT-GICD) using Neural Networks," *International Journal of Information Technology*, vol. 15, no. 7, pp. 3727-3739, 2023. [CrossRef] [Google Scholar] [Publisher Link]

[23] Krishnamoorthy Somasundaram, Paulraj Sivakumar, and Durairaj Suresh, "Classification of Diabetic Retinopathy Diseases with Transfer Learning using Deep Convolutional Neural Networks," *Advances in Electrical and Computer Engineering*, vol. 21, no. 3, pp. 49-56, 2021. [CrossRef] [Google Scholar] [Publisher Link]

[24] Maíla de Lima Claro et al., "Automatic Glaucoma Detection based on Optic Disc Segmentation and Texture Feature Extraction," *CLEI Electronic Journal*, vol. 19, no. 2, pp. 1-19, 2016. [CrossRef] [Google Scholar] [Publisher Link]

[25] Ryo Asaoka et al., "Detecting Preperimetric Glaucoma with Standard Automated Perimetry using a Deep Learning Classifier," *Ophthalmology*, vol. 123, no. 9, pp. 1974-1980, 2016. [CrossRef] [Google Scholar] [Publisher Link]

[26] Saad Albawi, Tareq Abed Mohammed, and Saad Al-Zawi, "Understanding of a Convolutional Neural Network," *2017 International Conference on Engineering and Technology (ICET)*, Antalya, Turkey, pp. 1-6, 2017. [CrossRef] [Publisher Link]

[27] Laith Alzubaidi et al., "Review of Deep Learning: Concepts, CNN Architectures, Challenges, Applications, Future Directions," *Journal of Big Data*, vol. 8, no. 1, pp. 1-74, 2021. [CrossRef] [Google Scholar] [Publisher Link]

[28] Ningning Ma et al., "ShuffleNetV2: Practical Guidelines for Efficient CNN Architecture Design," *Proceedings of the European Conference on Computer Vision (ECCV)*, Munich, Germany, 2018, pp. 116-131. [Google Scholar] [Publisher Link]

[29] Fu Huazhu et al., "Retinal Fundus Glaucoma Image Dataset," *Figshare*, 2023. [CrossRef] [Publisher Link]

[30] Laurent Massoptier, and Sergio Casciaro, "A New Fully Automatic and Robust Algorithm for Fast Segmentation of Liver Tissue and Tumors from CT Scans," *European Radiology*, vol. 18, no. 8, pp. 1658-1665, 2008. [CrossRef] [Google Scholar] [Publisher Link]

[31] Mahmoud Said Elsayed et al., "DDosNet: A Deep-Learning Model for Detecting Network Attacks," *2020 IEEE 21st International Symposium on A World of Wireless, Mobile and Multimedia Networks*, Cork, Ireland, pp. 391-396, 2020. [CrossRef] [Google Scholar] [Publisher Link]

[32] Xiao Chun Ling et al., "Deep Learning in Glaucoma Detection and Progression Prediction: A Systematic Review and Meta-Analysis," *Biomedicines,* vol. 13, no. 2, pp. 1-26, 2025. [CrossRef] [Google Scholar] [Publisher Link]

[33] Jiatong Zhang et al., "A Scoping Review of Advancements in Machine Learning for Glaucoma: Current Trends and Future Direction," *Frontiers in Medicine,* vol. 12, pp. 1-12, 2025. [CrossRef] [Google Scholar] [Publisher Link]

[34] Vibhanshu Gupta et al., *Glaucoma Detection in the Age of AI: A Solution for Sustainable Future*, 1st ed., CRC Press EBooks, pp. 528-534, 2025. [Google Scholar] [Publisher Link]

[35] K. Gogila Devi et al., "Machine Learning based Glaucoma Detection using Electroretinography (ERG) Signals for Early Diagnosis and Monitoring," *2025 7th International Conference on Inventive Material Science and Applications (ICIMA)*, India, pp. 436-441, 2025. [CrossRef] [Google Scholar] [Publisher Link]

[36] Malika Urazhanova et al., "Glaucoma Screening in Kazakhstan," *Scientific Reports,* vol. 15, no. 1, pp. 1-11, 2025. [CrossRef] [Google Scholar] [Publisher Link]

[37] Yukihiro Shiga et al., "*Editorial:* Advanced Ophthalmic Imaging in Glaucoma and other Optic Neuropathies," *Frontiers in Ophthalmology*, vol. 5, 2025. [CrossRef] [Google Scholar] [Publisher Link]

[38] Jalil Jalili et al., "Glaucoma Detection and Feature Identification via GPT-4V Fundus Image Analysis," *Ophthalmology Science*, vol. 5, no. 2, pp. 1-12, 2025. [CrossRef] [Google Scholar] [Publisher Link]